Asian Journal of Chemistry; Vol. 25, No. 1 (2013), 356-364

ASIAN JOURNAL OF CHEMISTRY

http://dx.doi.org/10.14233/ajchem.2013.13087

Structural Properties, Lattice Strain and Transformation of Anatase-Type TiO_2 Nanocrystals to Rutile in TiO_2-SiO_2 Composite

MEHRAN RIAZIAN, SHIMA DALIRI RAD, NASER MONTAZERI and KHALIL POURSHAMSIAN*

Department of Chemistry, Tonekabon Branch, Islamic Azad University, Tonekabon, Iran

*Corresponding author: E-mail: kh_pourshamsian@toniau.ac.ir

(*Received*: 23 November 2011; *Accepted*: 26 July 2012) AJC-11878

We report the synthesis of TiO_2 nanoparticles in anatase and rutile structures in SiO_2-TiO_2 composite. The SiO_2-TiO_2 nanostructure was synthesized based on the sol-gel method. The nanoparticles were characterized by X-ray fluorescents, X-ray diffraction, field emission scanning electron microscopy and Fourier transmission infrared absorption (FTIR) techniques. Phase formation was achieved by hydrothermal treatment at elevated temperatures. The anatase nanoparticles were obtained under 300 ºC calcined temperature, while rutile phase were obtained in higher than 300 ºC calcined temperature. The mass fraction of anatase and rutile phases was calculated. It can be fined that as the calcined temperature increases the per cent of rutile phase content grows, as well as when the content of TiO_2 in SiO_2-TiO_2 composite increases, the per cent of rutile phase content grows. The effects of chemical compositions and calcinations temperature on the surface topography and the crystallization of phases were studied.

Key Words: Nanostructure, Phase characterization, SiO_2-TiO_2, Sol-Gel method.

INTRODUCTION

Nanocrystalline materials are currently receiving much attention by virtue of their chemical, physical and mechanical properties. TiO_2 nanoparticles are gaining much attention due to crystal structure, nanoparticle size, morphology and the method of synthesis. TiO_2 has three naturally occurring polymorphous: anatase, rutile and brookite. Among them, the TiO_2 exists mostly rutile an anatase phases, which both of them have the tetragonal structures. However rutile is a high-temperature stable phase and has an optical energy band gap of 3 eV (415 nm), anatase is formed at lower temperature with an optical energy band gap of 3.2 eV (380 nm) and refractive index of 2.3[1].

The size of the TiO_2 particles is a considerable parameter that influences physical and chemical properties of materials, so that most of the recent researches have been focused upon the reaction of the particle size. The use and performance of mixed polymorphs in various applications are strongly influenced by the particle size, crystallite size, degree of crystallinity and morphology[2]. The anatase and rutile phases and phase transformation have been examined extensively. Many researchers intend to gather information on these phases and transition.

Among the many chemical techniques for the fabrication of materials, sol-gel processing as a moderate and adjustable method has emerged as an alternative route to control the size, morphology, structure and physical and chemical properties of inorganic oxides[3]. The sol-gel process is commonly applied to synthesize TiO_2 materials owing to its several advantages such as low temperature processing and the ability to prepare materials in various shapes, compared with the conventional preparation procedures of glass and ceramics[4,5]. In this study $TiCl_4$ and tetraethyl orthosilicate used as starting materials were hydrolyzed using CH_3COOH solution.

EXPERIMENTAL

In this work we prepare TiO_2 by using hydrolysis procedure of $TiCl_4$, which is transformed to anatase by heating it at 300, 500, 700 and 900 ºC. It obviously depends on the preparation procedures and TiO_2 content in combination. Anatase is generally transformed to rutile if calcinations temperature and TiO_2 content increase (Fig. 1). By adding more SiO_2 to TiO_2, the obtained powder trend to crystalline structure.

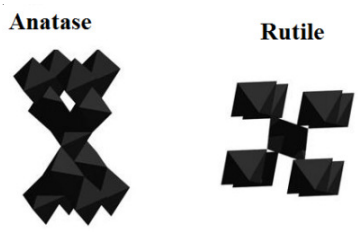

Fig. 1. Schematic model of anatase and rutile

The preparation of TiO_2-SiO_2 gel is below, such that tetraethyl-orthosilicate (TEOS) (Merk, ≥ 99 %) was hydrolyzed with deionized water in ethanol. Ethanol acts as a mutual solvent. Tetraethyl-orthosilicate, in ethanol was hydrolyzed with water containing acetic asid at room temperature for 0.5 h. The solution was then mixed with titanium chloride (Merk, at 0 ºC in specific molar ratio to obtain various content of TiO_2. After 30 min stirring at room temperature, the sol was vibrated for 20 min in ultrasonic bath to deconglomerate particles and then relaxed at room temperature for 30 min. The sol was stirred at 60 ºC until it become gel and removes ethanol (about 24 h). After gelation, samples were dried at 60 ºC to remove water and acetic acid and leave a white to light yellow lump depends on TiO_2 content. After that the lump samples were milled with mortar and calcinated in 300, 700 and 900 ºC. The thermal gradient during experiments procedure was 5 deg/min and the samples were put in oven during 2 h at calcination temperature stated above. The procedure was shown in Fig. 2. The corresponding molar ratios of TEOS-$TiCl_4$-Ethanol-H_2O-CH_3COOH are shown in Table-1 that A and B are molar ratio of TEOS and $TiCl_4$ composition. The weight per cent of ingredient in production was obtained by using XRF technique and given in Table-2.

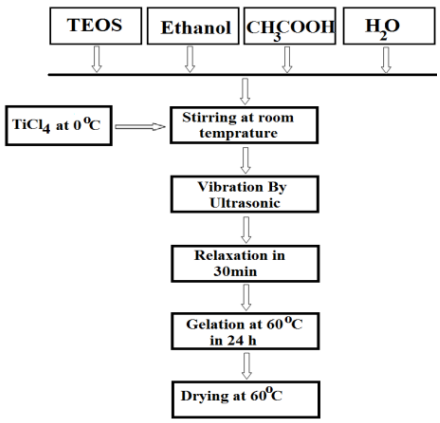

Fig. 2. Procedure for preparing TiO_2-SiO_2 in mixture

TABLE-1
MATERIALS AND CORRESPONDING MOLAR RATIO

Materials	TEOS	$TiCl_4$	Ethanol	H_2O	CH_3COOH
Symbol	A	B	C	D	E
Molar ratio	A	B	7(A+B)	10(A+B)	2(A+B)

TABLE-2
RESULT OF XRF ANALYSIS

Sample	Weight
100	70.75 % TiO_2-29.25 % SiO_2
200	59.43 % TiO_2-40.57 % SiO_2
300	54.94 % TiO_2-45.06 % SiO_2
400	44.1 % TiO_2-55.90 % SiO_2
500	33.88 % TiO_2-66.12 % SiO_2
600	31.76 % TiO_2-68.24 % SiO_2

X-ray powder diffraction study: X-ray powder diffraction (XRD) patterns were measured on a (GBC-MMA 007 (2000)) X-ray diffractometer. The diffractograms were recorded with [K_α(Cu), 1.54 Å, 0.02º step size in where the speed was 10 deg/min] radiation over a 2θ range of 10º - 80º.

Filed-emission electron microscopy: FE-SEM (S-4160 Hitachi) was routinely used to investigate the morphology of the nano-particles.

FT-IR study: FT-IR measurements were performed on a 1730 Infrared Fourier Transform Spectrometer (Perkin-Elmer) using the potassium bromide as the background.

RESULTS AND DISCUSSION

Two factors determine the hydrolysis and condensation rates. First factor is the acetic acid, which promote the hydrolysis of TEOS; the second is the titanate formed by the chelate of acetic acid and titanium, which accelerate the condensation of TEOS[5]. With respect to acetic acid, it plays two roles in the system. One side, it acts as the catalyst to promote the hydrolysis of TEOS; on the other side, it chelate with titanium to form titanate, which accelerate the condensation of TEOS and retard the hydrolysis and condensation of TIOT. In the present work, the TEOS is partially hydrolyzed in methanol, water and hydrochloric acid under controlled conditions that allow the solution, *i.e.*, sol, to yield a formable, loosely cross-linked matrix, *i.e.*, gel. Then, titanium chelate compound (PTP) was added to form polytitanosiloxane solution (TiSi) *via* polycondensation reaction [eqns.(1 and 5)]. TiO_2-SiO_2 precursor solution consists of siloxane (Si-O-Si) and Si-O-Ti linkages as a main chain.

Titanium alkoxide is hydrolyzed and condensed to form polymeric species composed of M-O-M bonds in butanol solution. The process is generally described in eqns. 2 and 4.

Hydrolyzing water can be supplied *via* two different mechanisms. The first mechanism is the esterification of ethanol and acetic *in situ*, as shown in eqn. 4. The second one is the oxolation, as shown in eqn. 3. The esterification product, butyl acetate was found and identified by a GC/Mass (HP GCD plus). The esterification becomes much more favourable when the ratio of acetic acid/metal alkoxide is low[6]. Acetic acid also serves as a chelating ligand and can change the alkoxide precursor at the molecular level, thus modifying the hydrolysis process[7]. Chelation can be described in eqn. 7 and 8. The hydrolysis of chelated titanium complex is deferred so that ethanol ligand may still remain in the sol. Upon further hydrolysis, ethanol ligand is broken off and gives to Ti-OH bond. This mechanism decreases the rate of hydrolysis, meaning very fine particles of titanium hydroxide will be formed and suspended in solution.

$$Si(OC_2H_5)_4 + nH_2O \xrightarrow[27\ ºC,\ 30\ min]{TEOS\quad HCl} Si(OC_2H_5)_n(OH)_n + nC_2H_5OH \quad (1)$$

$$Ti(OR)_4 + H_2O \rightarrow Ti(OR)_3(OH) + ROH \quad (2)$$

$$Ti(OR)_3(OH) + Ti(OR)_3(OH) \rightarrow (OR)_3Ti\text{-}O\text{-}Ti(OR)_3 + H_2O \quad (3)$$

$$Ti(OR)_3(OH) + Ti(OR)_4 \rightarrow (OR)_3Ti\text{-}O\text{-}Ti(OR)_3 + ROH \quad (4)$$

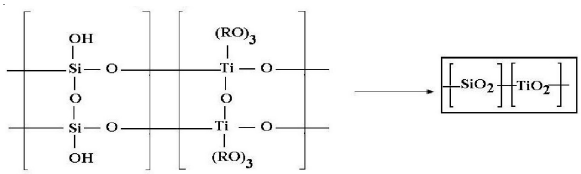

(5)

$$ROH + CH_3COOH \rightarrow H_2O + RCOOC_2H_2 \quad (6)$$

XRD patterns of nano-TiO_2 in rutile and anatase phases and their thermal treatment (calcined temperature) at 300, 500, 700 and 900 ºC are displayed in Figs. (3-13). Fig. (3-8) are the patterns of samples with specific TiO_2 content in TiO_2-SiO_2 composite, but different calcined temperatures. The position of all diffraction lines correspond to anatase and rutile phases are agreement with IU Cr reference database (99-100-9974) and (99-100-4865) card, respectively. The XRD patterns of the powder samples reveals the at 25º (101) and 48º (200) and rutile 27º (110), 36º (101), 55º (211), indicating that the samples are a mixture of anatase and rutile phases. The phase content of sample can be calculated from the integrated of anatase (101) at 25º and rutile (110) at 27º peaks. If samples contain anatase and rutile phases, the mass fraction of rutile (W_r) and anatase (W_a) can be calculated from $W_r = \frac{A_r}{0.886A_\alpha + A_r}$ and $W_\alpha = \frac{0.886A_\alpha}{0.886A_\alpha + A_r}$ that A_α and A_r represent the integrated intensity of the anatase (101) and rutile (110) peaks, respectively[9].

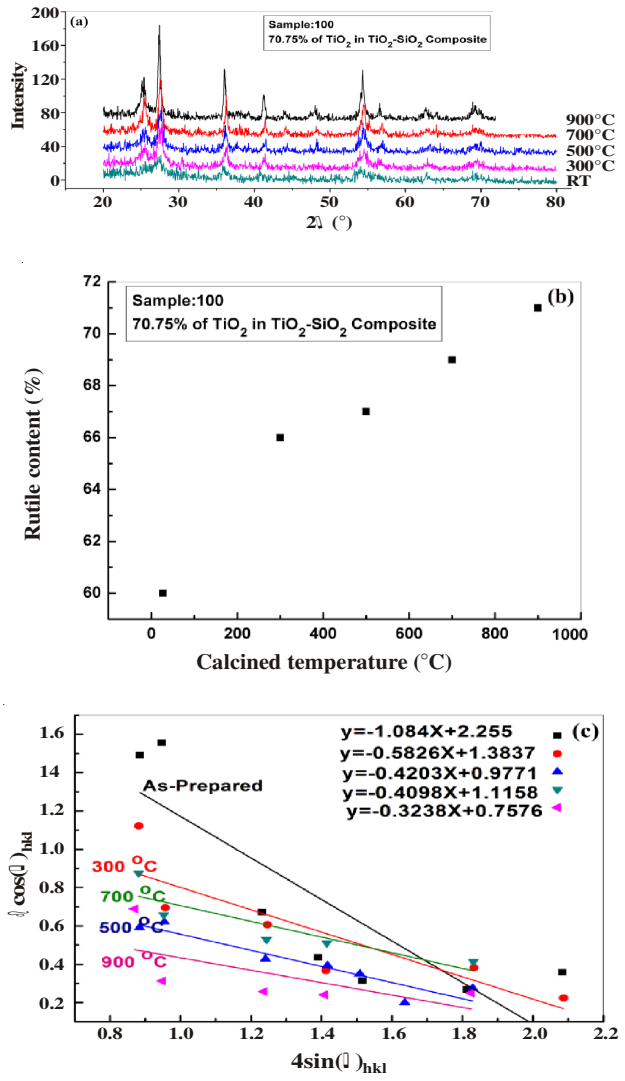

Fig. 3. (a) XRD patterns of the sample 100 correspond to content in Table-2 at different calcined temperature, (b) the per cent of rutile content per calcined temperature and (c) The linear relation between β cos θ and 4 sin θ (Williamson-Hall plots) for samples with different calcined temperatures

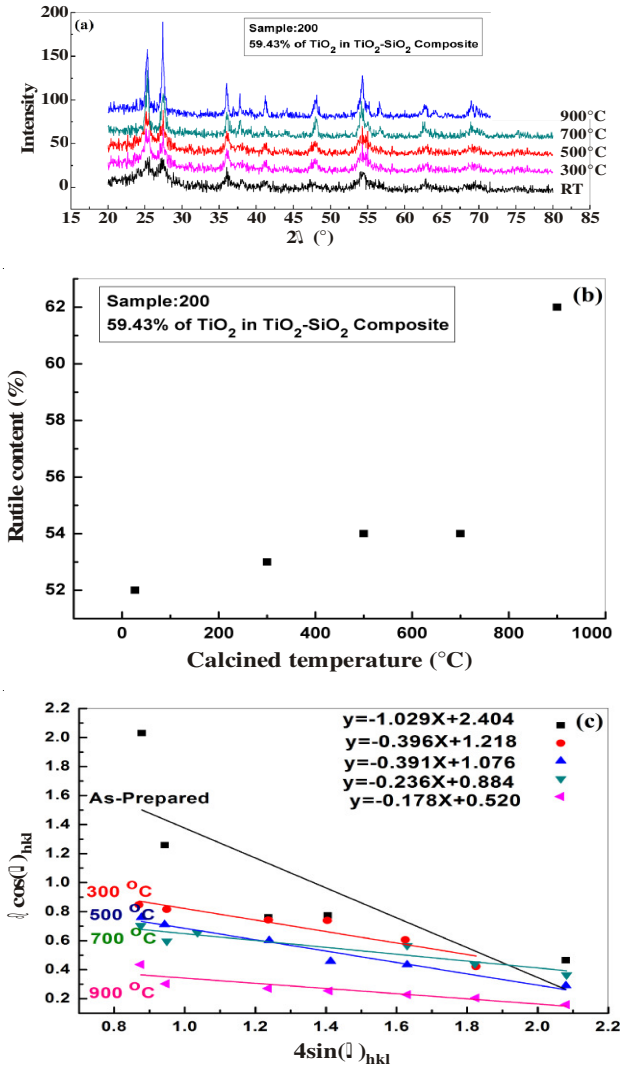

Fig. 4. (a) XRD patterns of the sample 200 correspond to content in Table- 2 at different calcined temperature, (b) the percent of rutile content per calcined temperature and (c) The linear relation between β cos θ and 4 sin θ (Williamson-Hall plots) for samples with different calcined temperatures

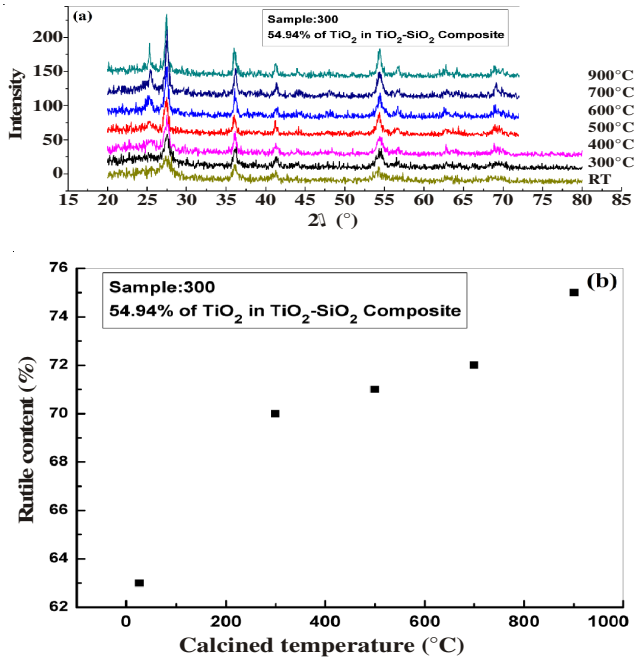

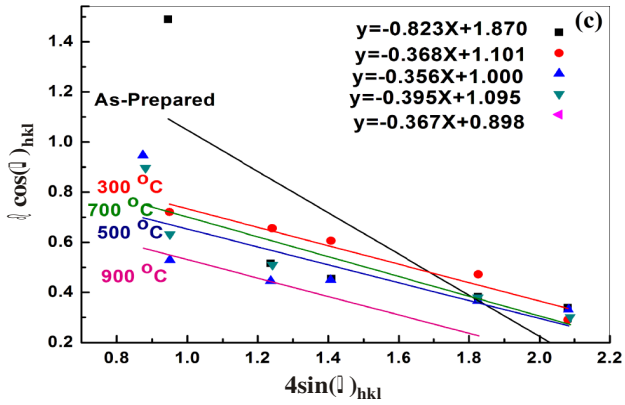

Fig. 5. (a) XRD patterns of the sample 300 correspond to content in Table- 2 at different calcined temperature, (b) the percent of rutile content per calcined temperature and (c) The linear relation between β cos θ and 4 sin θ (Williamson-Hall plots) for samples with different calcined temperatures

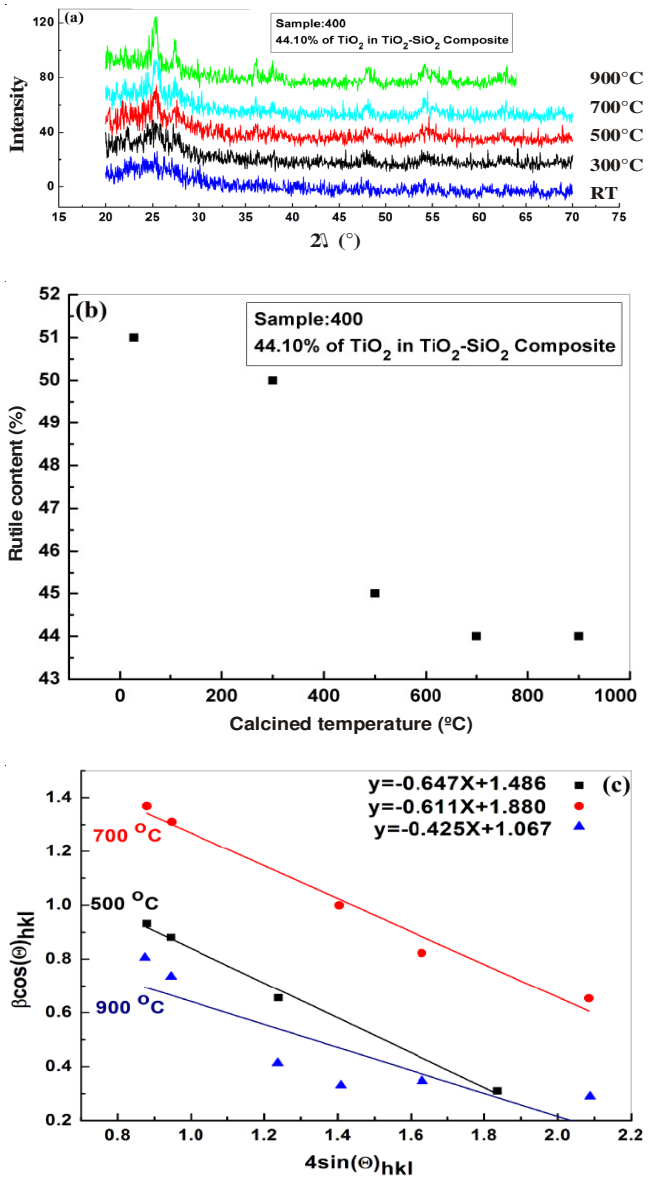

Fig. 6. (a) XRD patterns of the sample 400 correspond to content in Table- 2, at different calcined temperature, (b) the percent of rutile content per calcined temperature and (c) The linear relation between β cos θ and 4 sin θ (Williamson-Hall plots) for samples with different calcined temperatures

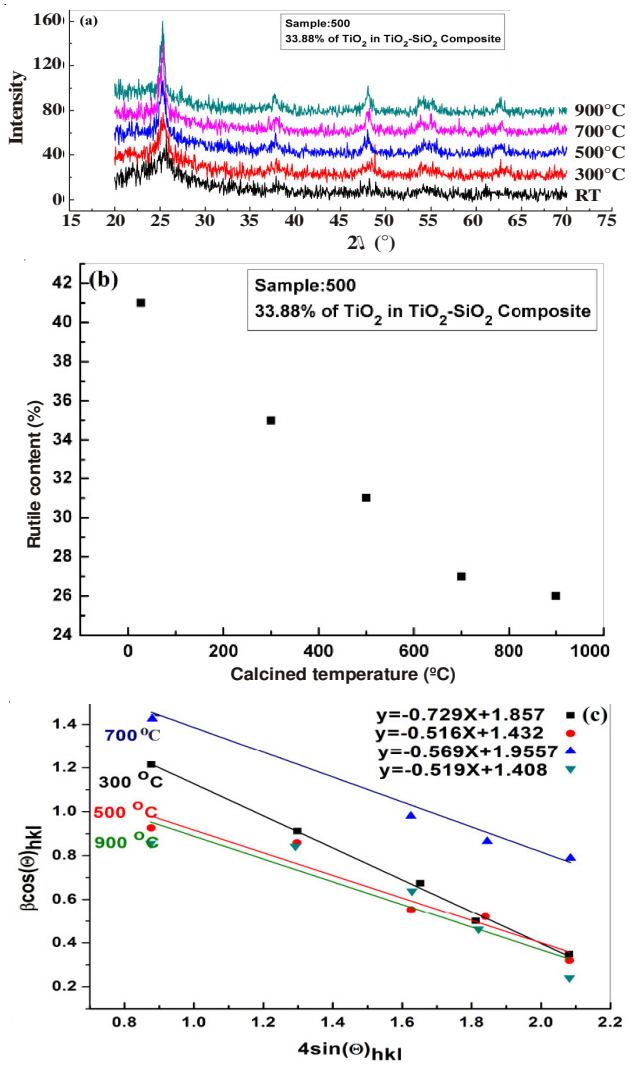

Fig. 7. (a) XRD patterns of the sample 500 correspond to content in Table- 2, at different calcined temperature, (b) the percent of rutile content per calcined temperature and (c) The linear relation between β cos θ and 4 sin θ (Williamson-Hall plots) for samples with different calcined temperatures

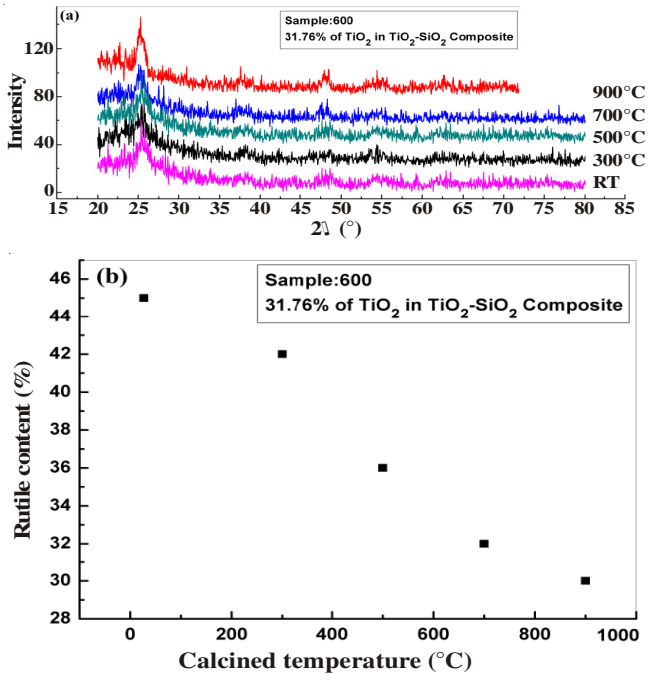

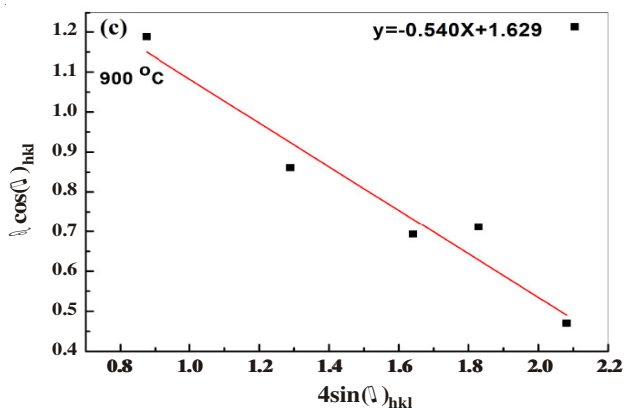

Fig. 8. (a) XRD patterns of the sample 600 correspond to content in Table-2, at different calcined temperature, (b) the percent of rutile content per calcined temperature and (c) The linear relation between β cos θ and 4 sin θ (Williamson-Hall plots) for sample with 900 ºC calcined temperature

In the samples with specific TiO_2 content, per cent of rutile content grows with increasing the calcined temperature, while with increasing the TiO_2 content in TiO_2-SiO_2 composite up to 44.1 % (after sample 400), the per cent of rutile content decreases with increasing the calcined temperature (Figs. 3-8). This manner is due to increasing the SiO_2 content in composite. Since the atomic radius of Si atom is smaller than Ti, the TiO_2 particle experience a contraction and its crystal growth is retarded duo to the Si atom.

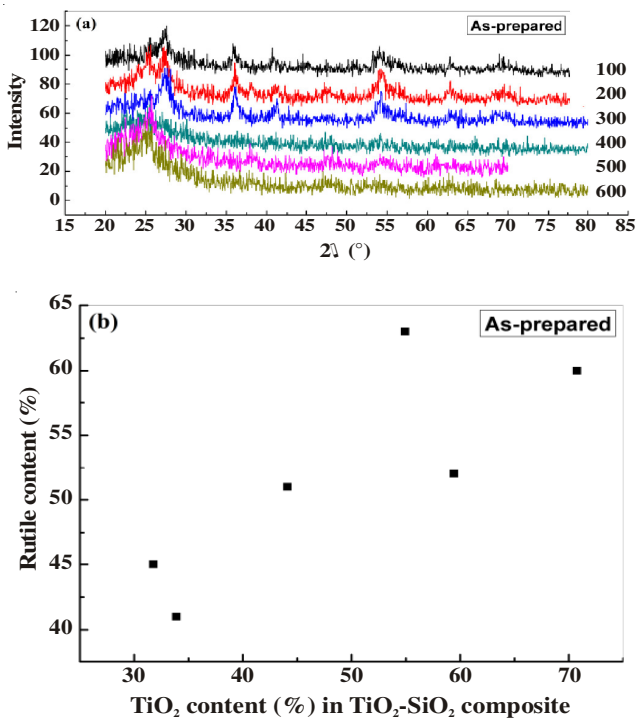

Fig. 9. (a) XRD patterns in as-prepared samples but different TiO_2 content and (b) the percent of rutile content per TiO_2 per cent content in composite. The inset table shows sample numbers correspond to TiO_2 content in Table-2

In the samples with specific calcined temperature, per cent of rutile content grows with increasing the TiO_2 content in TiO_2-SiO_2 composite (Figs. 9-13). In this case as the calcined temperature increases, the dispersal of data in schemes decreases so that the dotes can be fitted linearly (Figs. 9-13). From the data obtained of Scherer equation, it is observed that increasing of rutile and anatase nanocrystallite size was after calcined temperature (Table-3). There are no obvious realation between nanocrystalline size and percent of TiO_2 content in TiO_2-SiO_2 composite.

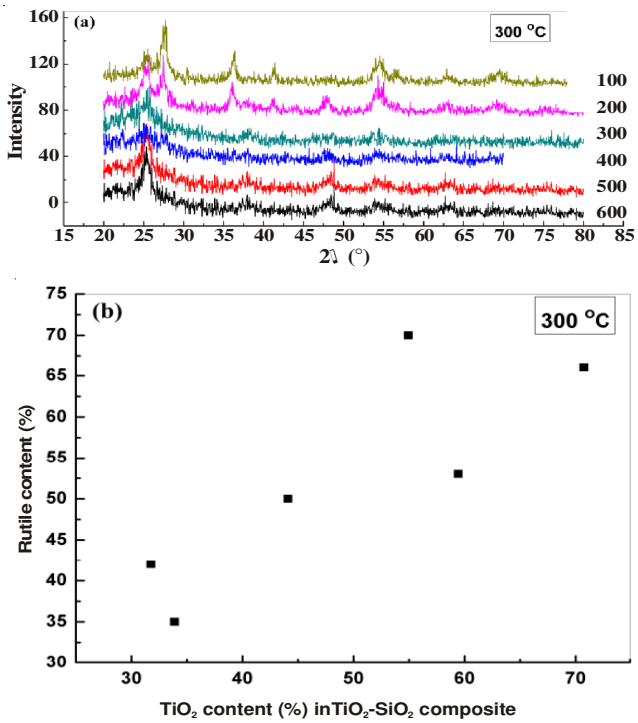

Fig. 10. (a) XRD patterns at fixed calcined temperature (300 ºC) but different TiO_2 content and (b) the per cent of rutile content per TiO_2 content. The inset table shows sample numbers correspond to TiO_2 content in Table-2

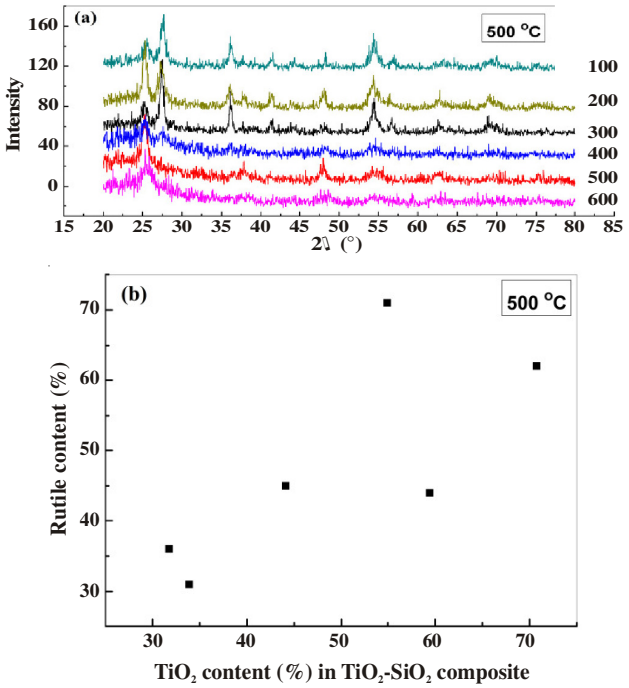

Fig. 11. (a) XRD patterns at fixed calcined temperature (500 ºC) but different TiO_2 content and (b) the per cent of rutile content per TiO_2 content. The inset table shows sample numbers correspond to TiO_2 content in Table-2

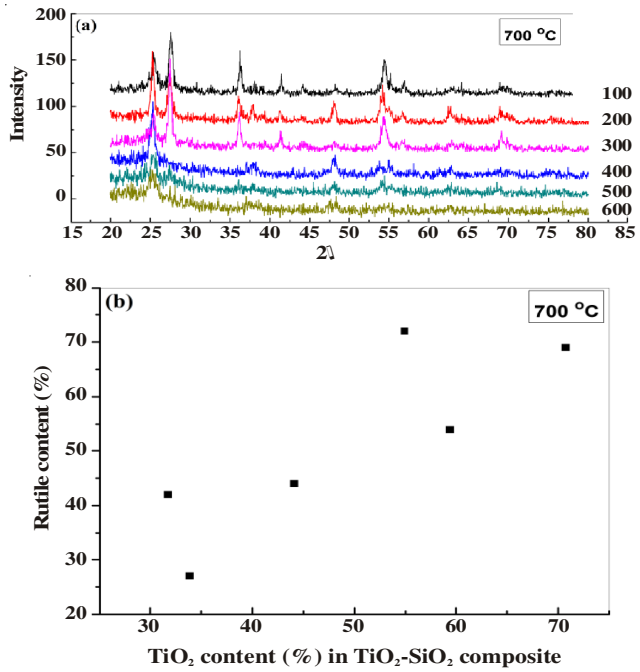

Fig. 12. (a) XRD patterns at fixed calcined temperature (700 °C) but different TiO_2 content and (b) the per cent of rutile content per TiO_2 content. The inset table shows sample numbers correspond to TiO_2 content in Table-2

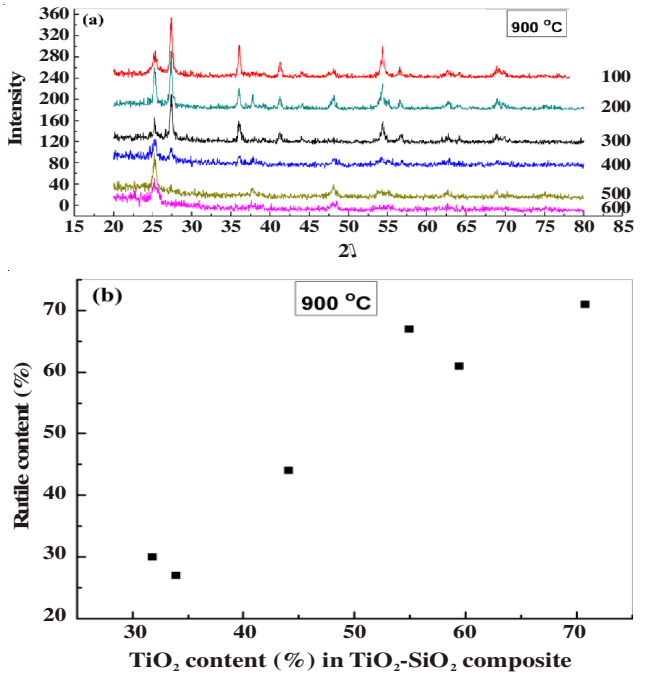

Fig. 13. (a) XRD patterns at fixed calcined temperature (900 °C) but different TiO_2 content and (b) the per cent of rutile content per TiO_2 content. The inset table shows sample numbers correspond to TiO_2 content in Table-2

TABLE-3
ANALYSIS OF XRD PATTERNS CORRESPOND TO TABLE-2. THE SIZE OF GRAIN IS DERIVED BY USING SCHERER'S EQUATION. THE PHASE IS ALSO EXTRACTED FROM DATABASE OF XRD PATTERNS (A= ANATASE, R= RUTILE). THE ANGLE (2θ) CORRESPONDS TO MORE INSENSITIVE PEAK RELEVANT TO ANATASE OR RUTILE PHASE

Temperature: As-prepared				Temperature: 300 °C			
Sample	Size (nm)	Phase anatase or rotile	Angle (2θ)	Sample	Size (nm)	Phase anatase or rotile	Angle (2θ)
100	6	R	27.40	100	8	A	25.40
					12	R	27.60
200	4	A	25.35	200	11	A	25.15
	7	R	27.35		24	R	27.45
300	6	R	27.35	300	8	R	27.50
400	3	A	25.20	400	8	A	25.50
					12	R	27.60
500	6	A	25.60	500	6	A	25.30
600	4	A	25.10	600	6	A	25.40
Temperature: 500 °C				Temperature: 700 °C			
Sample	Size (nm)	Phase anatase or rotile	Angle (2θ)	Sample	Size (nm)	Phase anatase or rotile	Angle (2θ)
100	16	A	25.50	100	10	A	25.40
	14	R	27.60		16	R	27.50
200	13	A	25.35	200	28	A	25.30
	10	R	27.30		16	R	27.45
300	9	A	25.25	300	10	A	25.45
	18	R	27.50		25	R	27.50
400	10	A	25.40	400	6	A	25.40
	8	R	27.35		7	R	27.40
500	10	A	25.30	500	13	A	25.35
600	7	A	25.35	600	4	A	25.30

Temperature: 900 °C			
Sample	Size (nm)	Phase anatase or rotile	Angle (2θ)
100	13	A	25.15
	33	R	27.45
200	23	A	25.30
	37	R	27.40
300	47	A	25.30
	30	R	27.45
400	13	A	25.25
	12	R	27.35
500	15	A	25.30
600	7	A	25.30

Lattice strain of nanocrystallites are determined from the dependence of FWHM of diffraction lines observed in 2θ range of 10-80 on sin θ, according to the Williamson-Hall's equation: $\beta\cos\theta = \frac{k\lambda}{L} + 4\sin\theta$ [10], where β was FWHM observed, shape factor k was assumed to be 0.9 similar to Scherrer equation's. λ (wavelength of K_α (Cu) were mentioned in 3-1. The plots of β cos θ against 4 sin θ for different samples were approximated to be linear. Lattice strain was determined from the slop of this linear relation. Because of low-crystallized powder samples, the linearity between β cos θ and 4 sin θ is not very evident[11]. The plots of β cos θ against 4 sin θ for different diffraction lines of anatase and rutile phases are illustrated in Figs. 3-8 and Table-4. For low calcined temperatures, the experimental points for the diffraction lines measured scattered, because the peaks are weak and broad so that their FWHMs were difficult to be measured. As shown in Fig. 14 for sample with specific TiO_2 content in composite, variation of lattice strain per calcined temperature and rutile content per calcined temperature are illustrated together. As can be seen in Figs. 3-8 and 14 and Table-4 in the specific TiO_2 content in composite, the lattice strain decreases with increasing the calcined temperature. Correspond to Figs. 14 and 15 for samples with more than 55 % of TiO_2 content in composite, the lattice strain

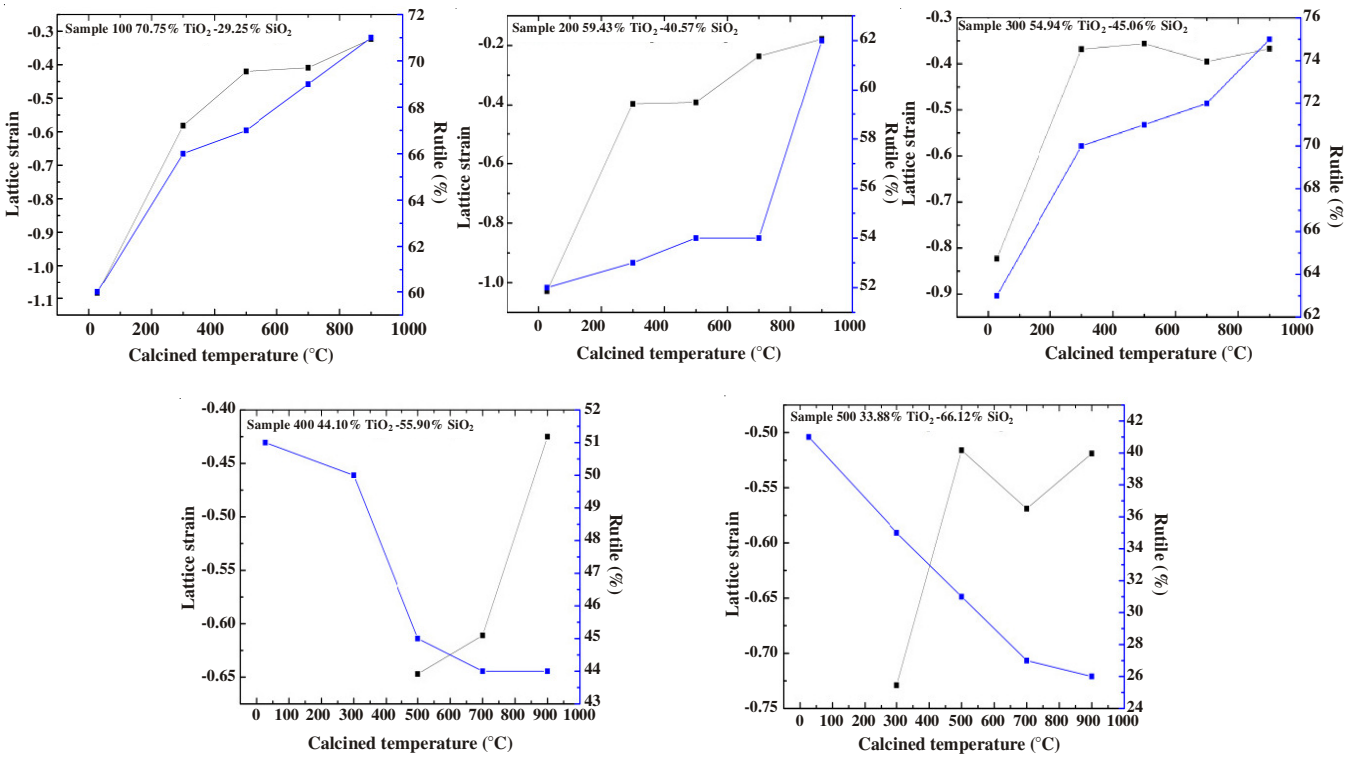

Fig. 14. Dependence of lattice strain and rutile content on calcined temperature

TABLE-4
LATTICE STRAIN AND RUTILE CONTENT OBTAINED IN DIFFERENT TiO_2 CONTENT IN COMPOSITE AND CALCINED TEMPERATURE

Sample and content of TiO_2			100 70.75 % TiO_2-29.25 % SiO_2		
Calcined Temperature °C	As-Prepared	300 °C	500 °C	700 °C	900 °C
Lattice Strain	-1.084	-0.582	-0.420	-0.409	-0.323
Percent of rutile (%)	60	66	67	69	71
Sample			200 59.43 % TiO_2-40.57 % SiO_2		
Lattice Strain	-1.029	-0.396	-0.391	-0.236	-0.178
Percent of rutile (%)	52	53	54	54	62
Sample			300 54.94 % TiO_2-45.06 % SiO_2		
Lattice Strain	-0.823	-0.368	-0.356	-0.395	-0.367
Percent of rutile (%)	63	70	71	72	75
Sample			400 44.1 % TiO_2-55.90 % SiO_2		
Lattice Strain	No linear relation	No linear relation	-0.647	-0.611	-0.425
Percent of rutile (%)	51	50	45	44	44
Sample			500 33.88 % TiO_2-66.12 % SiO_2		
Lattice Strain	No linear relation	-0.729	-0.516	-0.569	-0.519
Percent of rutile (%)	41	35	31	27	26
Sample			600 31.76 % TiO_2-68.24 % SiO_2		
Lattice Strain	No linear relation	No linear relation	No linear relation	No linear relation	-0.540
Percent of rutile (%)	45	42	36	32	30

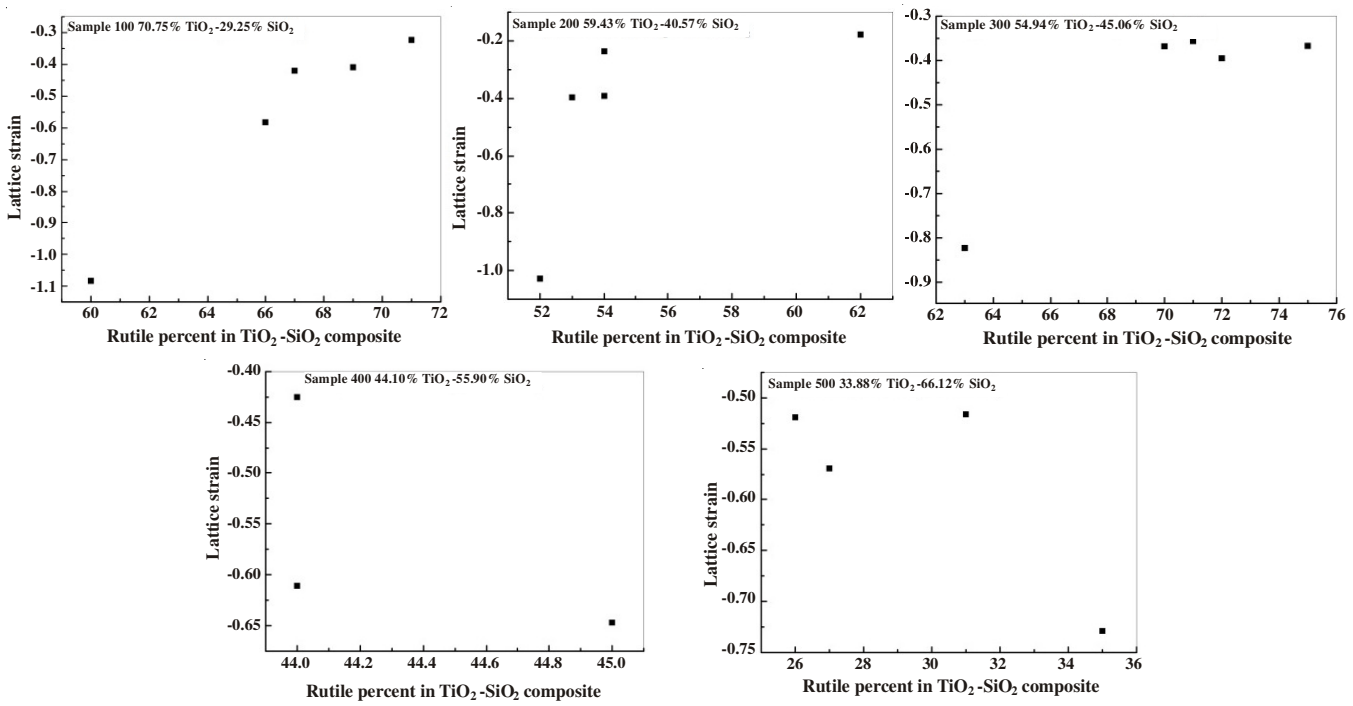

Fig. 15. Dependence of lattice strain on rutile content in composite

has a same behaviour as rutile content per calcned temperature. But for samples with less than 45 % of TiO_2 content, the lattice strain has a reverse behaviour with rutile content per calcined temperature. Our obtains are agreement with Inagaki[11] results that suggests the phase transformation from anatase to rutile structure is mainly governed by the lattice strain.

Fig. 16 shows FE-SEM pictures of the TiO_2-SiO_2 powder. This figure shows spherical and agglomerated TiO_2-SiO_2 nano-particle which was obtained using different molar ratios of reagents; the molar ratio of the solvent is also important. With a lower molar ratio of solvent (ethanol), agglomerated silica particles were obtained. Park and Kim[12] have shown when a narrow size distortion is required, a small molar ratio of ethanol should be employed. Nano-size of TiO_2-SiO_2 particles with spherical shape observed in specific condition. Spherical shape is obvious when calcination temperature and TiO_2 content in mixture increase compare to low content TiO_2 that cause random or dendrite shape in mixed oxides. The particle size grows relatively by increasing calcination temperature and TiO_2 content. This is due to the suppressive effect of SiO_2 on the crystal growth of TiO_2. This is accordance with the result of XRD analysis, which shows that the restriction of crystal growth of TiO_2 particles.

The FT-IR spectrum of TiO_2-SiO_2 consists of several bands at 1740, 1630, 1060-1220, 950, 798 and 740-650 cm^{-1}. The peaks in the spectra have been assigned according to the literature[13]. The bands at 1630 and 3300 cm^{-1} are assigned to OH bending and stretching vibrations respectively. It can be ascribed to the stretching of silanol groups interacting through hydrogen bonds with water molecules. The vibration in the range 1220-1060 cm^{-1} is assignable to Si-O-Si vibration mode of isolated Si-OH groups. The absorption band about 1070 cm^{-1} represents the characteristic bonds of Si-O-Si asymmetric stretching. The band near 950 cm^{-1} refers to Ti-O-Si asymmetric stretching. The peak near 798 cm^{-1} may be assigned to the O-Si-O vibration mode of SiO_2. The absorption band observed at about 950 cm^{-1} is associated with titanium in four-fold coordination with oxygen in the structure.

Other titanium-associated absorptions occur in broad bands at 400-240 cm^{-1} and 730-650 cm^{-1}. These lie just below the host-silica absorptions at 450 and 798 cm^{-1}. In spite of the result of Y. Zhao *et al.*[14], this band does not still in the spectrum after heating treatment at 600 ºC. We found that the intensity of the IR absorption peak is function of temperature and TiO_2 content. The prominent IR-active bands of pure silica are ascribed to TO modes of the SiO_4 network that have substantial motions of the light oxygen ions. These network modes involve vibrations of the bridging oxygen ions of corner-sharing SiO_4 tetrahedra. From this data, it is concluded that titanium is in four coordination with oxygen in the structure and each component in the materials is mixed on an atomic scale[15].

Conclusion

We report the synthesis of anatase and rutile nanoparticles by controlling the treatment temperature of the as-prepared sample. The homogeneous hydrolysis of metal alkoxide provided an excellent technique to prepare nanoparticle material. Experimental results indicated that the homogeneous hydrolysis of tetra isopropy ortho titanate and tetraethyl-orthosilicate *via* sol-gel route is a promising technique for preparing material with uniform nanoparticles. The effect of TiO_2-SiO_2 composite on the structural properties of powders prepared by sol-gel technique has been examined. In a two phases mixture of TiO_2 anatase transforms to rutile phase where size of anatase and rutile nanocrystaline were showed in Table-3. It was shown that with increasing the calined temperature, crystalline size increased. The mass fraction of anatase and rutile phases was calculated. It can be fined that as the calcined

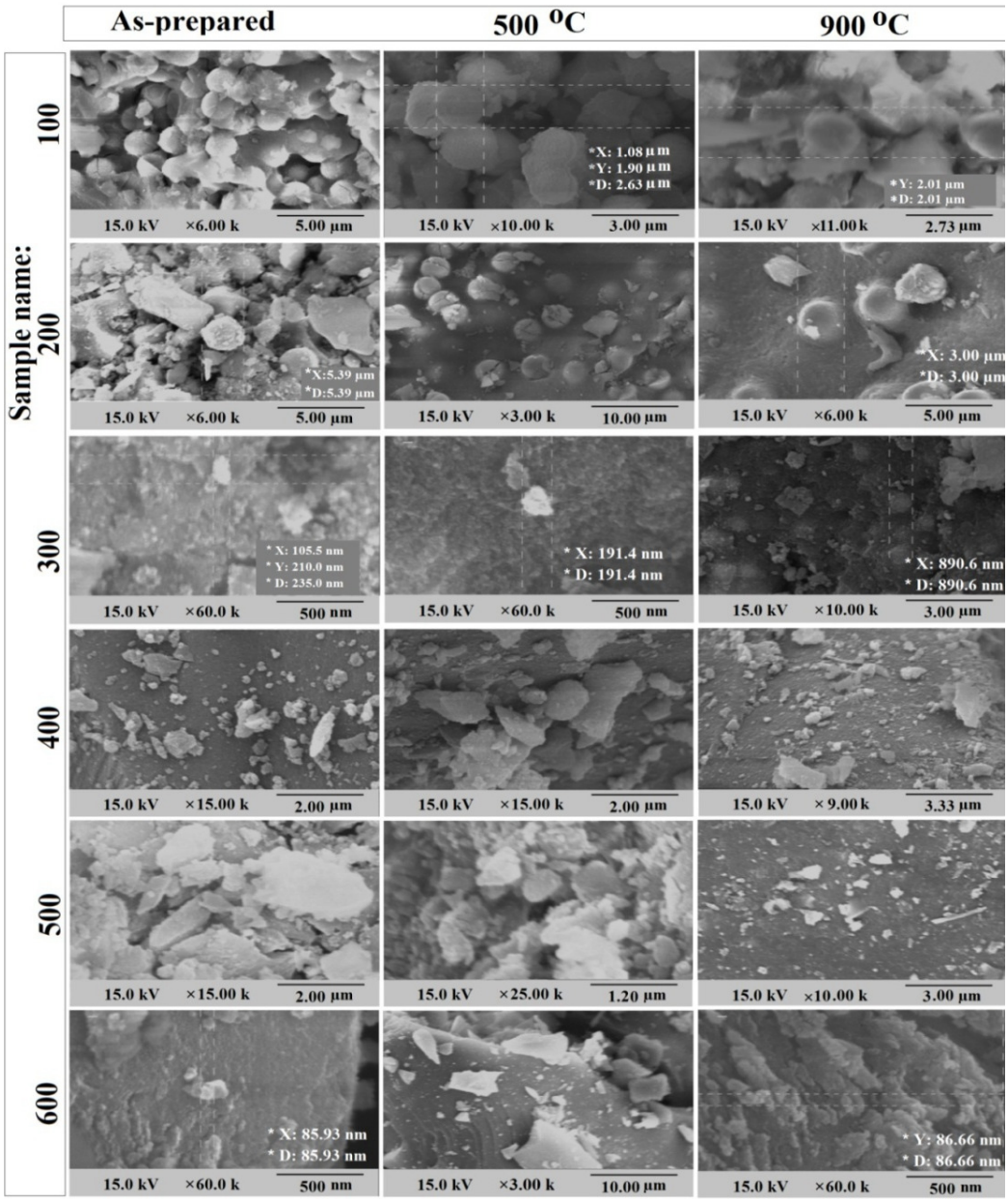

Fig. 16. FE-SEM images of the powder samples. Columns are found at calcined temperature and rows indicate the TiO_2 content in composite

temperature increases the percent of rutile phase content grows, as well as when the content of TiO_2 in SiO_2-TiO_2 composite increases, the per cent of rutile phase content grows. Lattice strain decreases with increasing the calcined temperature, accompanying the growth of nanocrystalline size. The scanning electron microscopy measurements showed nanostructure and morphology of powders. FTIR spectra of the ternary composite was presented and showed the possible bonds Si-O-Ti, Ti-O-Si, Ti-O-Ti, O-Si-O and Si-O-Si.

ACKNOWLEDGEMENTS

The authors thank Islamic Azad University, Tonekabon branch for financial support through a research project.

REFERENCES

1. K. Thamaphat, P. Limsuwan and B. Ngotawornchai, *J. Nat. Sci.*, **42**, 357 (2008).
2. S. Bakardjieva, V. Stengl, L. Szatmary, J. Subrt, J. Lukac, N. Murafa, D. Niznansky, K. Cizek, J. Jirkovsky and N. Petrova, *J. Mater. Chem.*, **12**, 1710 (2006).
3. Y. Yin and A.P. Alivisatos, *Nature*, **437**, 664 (2005).
4. K. Kato, A. Tsuzuki, H. Taoda, Y. Torii, T. Kato and Y. Butsugan, *J. Mater. Sci.*, **29**, 5911 (1994).
5. Y. Abe, N. Sugimoto, Y. Nagao and T. Misono, *J. Non-Cryst. Solids*, **104**, 164 (1988).
6. J.H. Lee, S.Y. Choi and C.E. Kim, *J. Mater. Sci.*, **32**, 3577 (1997).
7. S. Doeuff, M. Henry and C. Sanchez, *Mater. Res. Bull.*, **25**, 1519 (1990).
8. S. Doeuff, M. Henry, C. Sanchez and J. Livage, *J. Non-Cryst. Solids*, **89**, 206 (1987).
9. H. Zhang and J.F. Banfdield, *J. Phys. Chem. B.*, **104**, 3481 (2000).
10. O. Carp, C.L. Huisman and A. Reller, *Prog. Solid State Chem.*, **32**, 177 (2004).
11. M. Inagaki, R. Nonaka, B. Tryba and A.W. Morawski, *Chemosphere*, **64**, 437 (2006).
12. S.K. Park and K.D. Kim, *Coll. Surf. Sci.*, **78**, 197 (2002).
13. H.F. Yu and S.M. Wang, *J. Non-Cryst. Solids*, **261**, 260 (2000).
14. Y.X. Zhao, L.P. Xu, Y.Z. Wang, C.G. Gao and D.S. Liu, *Catal. Today*, **93-95**, 583 (2004).
15. A.A. Gribb and J.F. Banfield, *Am. Mineral.*, **82**, 717 (1997).